THEORETICAL ELUCIDATION OF THE ZOLEDRONIC ACID–B-CYCLODEXTRIN INCLUSION COMPLEX: A MULTI-LEVEL ANALYSIS USING DOCKING, NCI, QTAIM, NMR, NBO, AND TD-DFT METHODS

WAHIBA BOUNEB,[*,**] ABDELAZIZ BOUHADIBA,[*] AMINA BENAISSA,[***] NOURA NAILI,[****,*****] MOHAMED RAHIM,[*] YOUGHOURTA BELHOCINE[*] and HASSINA CHEKROUD[**,******]

[*]*Laboratory of Catalysis, Bioprocess and Environment, Department of Process Engineering, Faculty of Technology, University of 20 August 1955, Skikda 21000, Algeria*
[**]*LRPCSI-Laboratoire de Recherche sur la Physico-Chimie des Surfaces et Interfaces, University of 20 August 1955, Skikda 21000, Algeria*
[***]*Laboratory of Génie Chimique Et Environnement de Skikda (LGCES), Department of Process Engineering, Faculty of Technology, 20 Août 1955 University, P.O. Box 26, 21000, Skikda, Algeria*
[****]*Unité de Recherche de Chimie de L'Environnement Et Moléculaire Structurale (CHEMS), University Constantine (Mentouri), 25000, Constantine, Algeria*
[*****]*Department of Chemistry, Faculty of Science, 20 Août 1955 University, P.O. Box 26, 21000, Skikda, Algeria*
[******]*Department of Petrochemistry and Process Engineering, Faculty of Technology, University August 20, 1955-Skikda, BP 26 Route El Hadaik, Skikda, 21000, Algeria*
✉ *Corresponding author: Y. Belhocine, y.belhocine@univ-skikda.dz*

Received October 18, 2025

This study examines the inclusion complexation of zoledronic acid (ZA) with β-cyclodextrin (β-CD) using advanced computational approaches. Density Functional Theory (DFT) calculations with Grimme's D3 dispersion correction were employed to investigate the molecular structure, stability, non-covalent interactions, and thermodynamic properties of the complex in both gas phase and aqueous solution. The results demonstrate that the inclusion of ZA into the β-CD cavity is thermodynamically favorable, with the most stable configuration identified as configuration A, in which the imidazole moiety of ZA enters through the wider rim of the β-CD. Although solvation in water slightly decreases the overall stability of the complex, it does not significantly hinder its favorable formation. Non-covalent interactions, including hydrogen bonding and van der Waals forces, were analyzed using Natural Bond Orbital (NBO) analysis and the Quantum Theory of Atoms in Molecules (QTAIM). The findings highlight the crucial role of electrostatic interactions in stabilizing the complex, especially in the aqueous phase. Furthermore, NCI-RDG and IGM analyses were conducted to investigate van der Waals contacts, hydrogen bonding, and steric repulsion. Time-Dependent DFT (TD-DFT) calculations were also performed to simulate visible absorption spectra. Nuclear Magnetic Resonance (NMR) chemical shift calculations were carried out to compare theoretical predictions with experimental data, providing additional support for the encapsulation mechanism. Monte Carlo (MC) simulations were used to explore the conformational flexibility and dynamic behavior of the ZA@β-CD complex. These theoretical insights contribute to a deeper understanding of ZA@β-CD inclusion complexes and support the design of pharmaceutical formulations aimed at enhancing drug solubility and bioavailability.

Keywords: zoledronic acid, β-cyclodextrin, inclusion complex, DFT, non-covalent interactions

INTRODUCTION

Zoledronic acid (ZA) is a highly potent, nitrogen-containing bisphosphonate extensively used in the treatment of bone-related disorders, such as osteoporosis and metastatic bone disease.[1-3] Its therapeutic efficacy is attributed to its strong affinity for hydroxyapatite in bone tissue and its inhibition of osteoclast-mediated bone resorption through the targeting of farnesyl diphosphate synthase, a key enzyme in the mevalonate

pathway.[4,5] Despite its clinical benefits, the oral administration of ZA is significantly hindered by its low gastrointestinal absorption and high acidity, leading to poor bioavailability and potential adverse effects, including mucosal irritation and esophageal complications during long-term therapy.[6,7]

To overcome these limitations, the formation of inclusion complexes with β-cyclodextrin (β-CD) has emerged as a promising pharmaceutical strategy. β-CD is a cyclic oligosaccharide recognized for its capacity to encapsulate hydrophobic molecules within its nonpolar cavity, thereby enhancing the solubility, stability, and pharmacokinetic profiles of various therapeutic agents.[8,9] This work is intended to provide a comprehensive confirmation and in-depth characterization of the inclusion complex formed between ZA and β-cyclodextrin. Through the application of advanced theoretical methods, including DFT calculations with GIAO, it aims to offer robust evidence of host–guest interactions, as corroborated by NMR spectral data.[9]

Building on these experimental findings, the present study aims to deepen the understanding of the ZA@β-CD inclusion complex through theoretical modeling. Density Functional Theory (DFT) calculations, incorporating Grimme's D3 dispersion correction, were employed to investigate the molecular geometry, non-covalent interactions, and electronic properties of the complex.[10–14] Additionally, complementary theoretical techniques such as Quantum Theory of Atoms in Molecules (QTAIM) and Natural Bond Orbital (NBO) analysis were utilized to provide further insights into the stabilization mechanisms within the host–guest system.

To comprehensively characterize the intermolecular interactions within the complex, both visual and energetic descriptors, such as the Reduced Density Gradient (RDG) and Independent Gradient Model (IGM), were employed, allowing for a detailed visualization of hydrogen bonding and van der Waals forces. Furthermore, time-dependent DFT (TD-DFT) calculations were conducted to investigate the excited-state properties and potential photophysical behaviors of the system. Monte Carlo (MC) simulations complement these studies by assessing conformational flexibility and thermodynamic stability. Finally, theoretical NMR chemical shifts, computed via the Gauge-Including Atomic Orbital (GIAO) method, were compared to the experimental NMR data, providing validation of the proposed structural models and ensuring consistency between theoretical predictions and empirical findings.

EXPERIMENTAL

Computational details

All quantum chemical calculations were performed using the Gaussian 09W software package,[15] and molecular visualizations were generated with GaussView 6.[16] The initial structure of ZA was constructed using HyperChem 7.5.[17] The initial geometry of β-cyclodextrin was constructed directly in three-dimensional form using the ChemOffice 3D Ultra molecular builder (CambridgeSoft).[18] This structure was used as a starting geometry for subsequent calculations. Preliminary geometry optimizations for both the isolated molecules and their inclusion complexes were carried out using the semi-empirical PM6-D3H4 method, as implemented in MOPAC2016,[19] which incorporates dispersion and hydrogen-bond corrections for improved accuracy.

To systematically identify the most stable configuration of the ZA@β-CD inclusion complex, the protocol established by Liu *et al.*[20] was followed. Two initial orientations were considered: Configuration A, in which the imidazole ring of ZA enters through the wider rim of the β-CD cavity, and configuration B, where the phosphonate groups are inserted from the same side (Fig. 1). The configuration yielding the lowest total energy was selected for subsequent analyses.

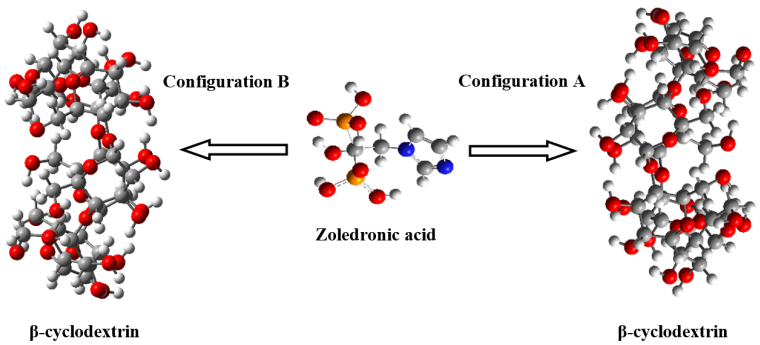

Figure 1: Coordinate systems describing the complexation process for A and B modes

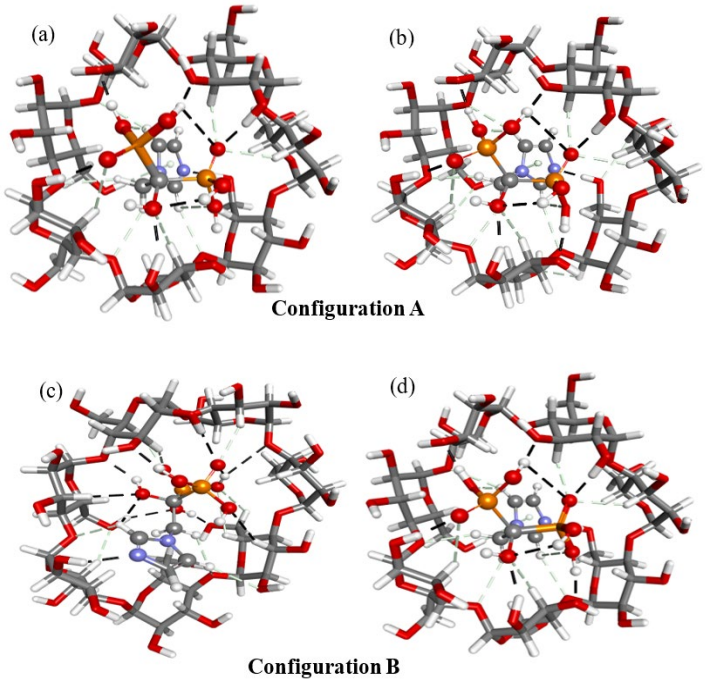

Figure 2: Optimized ZA@β-CD complexes (Configurations A and B) in the gas phase (a, c) and in aqueous solution (b, d), obtained using the B3LYP-D3/6-31G(d,p) method

The complexation energy ($E_{complexation}$) was calculated using Equation (1):

$$E_{Complexation} = E_{ZA@\beta\text{-}CD} - (E_{freeZA} + E_{free\beta\text{-}CD}) \quad (1)$$

where $E_{ZA@\beta\text{-}CD}$, E_{freeZA} and $E_{free\beta\text{-}CD}$ represent the total energies of the complex, the isolated guest, and the isolated host, respectively.

To accurately characterize the electronic structure and energetic properties of the studied systems, Density Functional Theory (DFT) calculations were carried out using the B3LYP functional augmented with Grimme's D3 empirical dispersion correction (B3LYP-D3),[21,22] in combination with the 6-31G(d,p) basis set.[23] Geometry optimizations were performed both in the gas phase and in aqueous solution, with solvation effects modeled via the Conductor-like Polarizable Continuum Model (CPCM).[24] This level of theory has been widely validated for its ability to describe non-covalent interactions, including hydrogen bonding and van der Waals forces, which are critical in host–guest chemistry.

Harmonic vibrational frequency calculations were conducted to verify the nature of the optimized geometries as true minima and to obtain thermodynamic corrections. To further explore the chemical reactivity and stability of the inclusion complexes, frontier molecular orbital (FMO) analysis was performed. The energies of the highest occupied molecular orbital (HOMO) and the lowest unoccupied molecular orbital (LUMO) were used to compute global reactivity descriptors,[25] including the HOMO–LUMO gap (ΔE), dipole moment (μ), chemical hardness (η), and electrophilicity index (ω).

A combination of complementary theoretical approaches was employed to characterize and visualize the intermolecular interactions within the ZA@β-CD inclusion complex. These included the Independent Gradient Model (IGM),[26,27] Natural Bond Orbital (NBO) analysis,[28,29] Non-Covalent Interaction (NCI) analysis combined with Reduced Density Gradient (RDG) methods,[30,31] and the Quantum Theory of Atoms in Molecules (QTAIM).[32] Together, these approaches enabled detailed identification of key interaction types, including hydrogen bonding, dispersion forces (van der Waals), and steric repulsion, thereby elucidating the nature and strength of host–guest interactions.

Theoretical proton chemical shifts (^{1}H NMR) were calculated using the Gauge-Including Atomic Orbital (GIAO) method,[33] and the resulting spectra were directly compared with experimental NMR data to validate the predicted complex structures. Post-processing of the IGM, NCI-RDG, and QTAIM analyses was performed using the Multiwfn program,[34,35] while graphical representations were generated with VMD software[36] for enhanced visualization of interaction regions.

The Monte Carlo (MC) docking simulations were carried out using HyperChem 7.5 with the AMBER99 force field, an implementation of the AMBER methodology developed by the Kollman group.[37–40] Although originally parameterized for biomacromolecules such as proteins and nucleic acids, AMBER99 has been widely validated for complex supramolecular systems, including carbohydrates and

cyclodextrin inclusion complexes such as γ-CD:C60.[37,39] A total of 500,000 configurations were generated to ensure exhaustive conformational sampling. Convergence was rigorously assessed based on energetic and structural stability, and was achieved when the energy variation between successive accepted configurations was <0.01 kcal·mol^{-1} and the maximum atomic displacement remained below 0.05 Å, ensuring reliable identification of the most stable inclusion geometry.

RESULTS AND DISCUSSION

Structural validation of the optimized β-cyclodextrin geometry

To assess the reliability of the optimized β-cyclodextrin (β-CD) structure, a comparative analysis was conducted against the experimental X-ray crystallographic data (CCDC 762697),[41] using least-squares superposition of heavy atoms (C and O). The root-mean-square deviation (RMSD) values obtained (2.74 Å) in the gas phase and (2.76 Å) under the CPCM solvation model, indicate good agreement with the experimental structure, particularly in light of the inherent conformational flexibility of the β-CD macrocycle and the influence of crystal packing effects. Furthermore, the calculated mean C–C and C–O bond distances closely reproduce the experimental values, indicating that the fundamental structural characteristics of β-cyclodextrin are accurately retained, despite the absence of intermolecular interactions in the computational model.

Complexation energies and thermodynamic parameters

This study evaluated the binding energetics of the ZA@β-CD inclusion complex by exploring two distinct spatial configurations, initially optimized using the semi-empirical PM6-D3H4 method. Subsequent re-optimization at the DFT level was performed to identify the most stable geometries. The results demonstrated that the encapsulation of ZA within the β-cyclodextrin cavity is thermodynamically favorable in both configurations, as indicated by the negative binding energies.

For configuration A, the global energy minimum was located at a translational coordinate of Z = 4 Å, with a binding energy of −76.77 kcal/mol. In contrast, configuration B exhibited its most stable geometry at Z = 6 Å, with a slightly less favorable binding energy of −75.39 kcal/mol. The 1.38 kcal/mol difference in favor of configuration A indicates superior thermodynamic stability (Table 1). These findings were further corroborated by DFT calculations at the B3LYP-D3/6-31G(d,p) level of theory (Table 2), which consistently supported the enhanced stability of configuration A.

Table 1
Complexation energies (in kcal/mol) of ZA@β-CD calculated at the PM6-D3H4 level

Z-axis (Å)	ZA@β-CD	
	Configuration A	Configuration B
-8	-42.94	-50.27
-7	-43.04	-50.30
-6	-41.31	-28.37
-5	-36.71	-53.92
-4	-46.89	-49.22
-3	-	-58.69
-2	-54.94	-55.45
-1	-63.88	-58.07
0	-53.06	-63.71
1	-61.61	-51.97
2	-46.33	-60.86
3	-50.42	-58.48
4	<u>-76.77</u>	-62.92
5	-30.80	-64.10
6	-70.09	<u>-75.39</u>
7	-60.33	-41.37
8	-67.13	-41.31

Table 2
Complexation energies, thermodynamic parameters, frontier molecular orbitals and electronic parameters for the inclusion of ZA with β-CD calculated at B3LYP-D3/6–31G (d, p)

Energetic terms	DFT-B3LYP-D3			
	In vacuum/In water (CPCM configuration)			
	ZA	β-CD	Configuration A	Configuration B
E (kcal/mol)	-951015.03/-951028.89	-2683056.57/-2683086.62	-3634143.44/-3634179.22	-3634139.23/-3634171.42
ΔE (kcal/mol)			-71.536/-64.006	-67.771/-55.848
H° (kcal/mol)	-950889.12/-950903.27	-2682240.77/-2682273.01	-3633199.23/-3633237.39	-3633194.62/-3633229.55
ΔH° (kcal/mol)			-69.330/-61.116	-64.724/-53.274
S° (Cal/mol-Kelvin)	127.633/128.689	381.437/386.319	435.311/437.163	440.026/447.458
ΔS° (Cal/mol-Kelvin)			-73.759/-77.845	-69.044/-67.550
G° (kcal/mol)	-950927.18/-950941.64	-2682354.50/-2682388.19	-3633329.01/-3633367.73	-3633325.81/-3633362.96
ΔG° (kcal/mol)			-47.338/-37.907	-44.138/-33.133
E_{HOMO} (eV)	-6.671/-6.572	-7.108/-7.061	-6.492/-6.616	-6.736/-6.585
E_{LUMO} (eV)	-0.119/0.004	1.093/1.326	-0.097/0.035	-0.169/-0.106
$\Delta E_{\lvert HOMO-LUMO \rvert}$ (eV)	6.552/6.569	8.201/8.387	6.395/6.650	6.567/6.479
μ (eV)	-3.395/-3.288	-3.007/-2.867	-3.295/-3.291	-3.453/-3.345
η (eV)	3.276/3.284	4.100/4.194	3.198/3.325	3.283/3.240
ω (eV)	1.759/1.646	1.103/0.980	1.697/1.628	1.815/1.727

Incorporation of solvation effects via the CPCM model revealed a notable reduction in binding energies for both configurations, attributed to the attenuation of non-covalent interactions in the aqueous phase. However, the process remained spontaneous, as indicated by negative standard Gibbs free energy values (ΔG°). For configuration A, ΔG° decreased from −47.34 kcal/mol in the gas phase to −37.91 kcal/mol in aqueous solution (Table 2), reflecting diminished, yet favorable, thermodynamic stability under solvation.

Standard enthalpy changes (ΔH°) were negative for all systems, confirming that complex formation is exothermic. Configuration A again exhibited a more favorable enthalpic contribution (−69.33 kcal/mol) compared to configuration B (−64.72 kcal/mol) in the gas phase, though this advantage was partially diminished in solution due to solvent-mediated disruption of intermolecular forces. Additionally, standard entropy changes (ΔS°) were negative in all cases, consistent with the reduced configurational freedom of the guest molecule upon encapsulation within the host cavity (Table 2).

Frontier Molecular Orbitals (FMO) and electronic properties

Frontier Molecular Orbital (FMO) analysis was performed to investigate the electronic structure and reactivity of the ZA@β-CD inclusion complexes. The results revealed notable differences between configurations A and B, particularly in their HOMO–LUMO energy gaps. In the gas phase, configuration A exhibited a narrower gap (6.395 eV) compared to configuration B (6.567 eV), indicating higher chemical reactivity and enhanced electronic stability for configuration A.

Further comparison of individual orbital energies showed that configuration A possessed a slightly higher HOMO energy (−6.492 eV) than configuration B (−6.736 eV), suggesting a greater tendency to donate electrons. Conversely, configuration B had a lower LUMO energy (−0.169 eV) relative to configuration A (−0.097 eV), implying an enhanced ability to accept electrons (Table 2). These electronic descriptors support the overall thermodynamic preference for configuration A, as observed in the binding energy analysis.

Global reactivity descriptors were calculated to further elucidate the electronic properties of the ZA@β-CD inclusion complexes. The chemical potential (μ), which indicates the tendency of electrons to escape from a system, was negative for both configurations, consistent with electronically stable systems. Configuration B exhibited a slightly more negative chemical potential (−3.453 eV) compared to configuration A (−3.295 eV), suggesting marginally greater electronic stability.

The global hardness (η), representing the system's resistance to charge transfer, was slightly higher for configuration B (3.283 eV) than for configuration A (3.198 eV), indicating lower chemical reactivity for the former. Additionally, the electrophilicity index (ω), which reflects the system's ability to accept electrons, was more pronounced in configuration B (1.815 eV) than in A (1.697 eV), supporting its slightly more electrophilic nature.

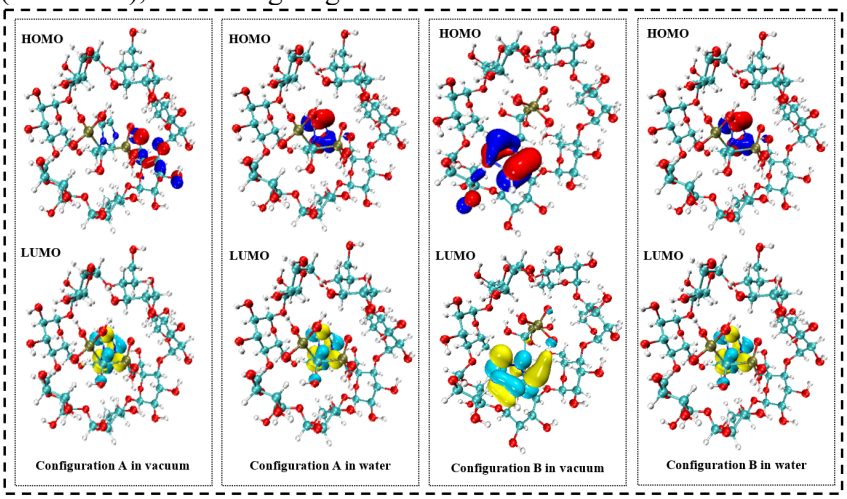

Figure 3: Typical contour plots of frontier molecular orbitals for the two configurations A and B obtained at B3LYP-D3/6–31G(d,p) in vacuum and water

Non-covalent intermolecular interactions

NBO analysis

Natural Bond Orbital (NBO) analysis was employed to investigate the donor–acceptor interactions that contribute to the stabilization of the ZA@β-CD inclusion complex. The calculations, performed at the B3LYP-D3/6-31G(d,p) level of theory, were conducted in both the gas phase and aqueous solution. The NBO analysis quantified second-order stabilization energies (E^2), which provide insight into the strength of electron donation and acceptance within the system.

The results (Table 3) revealed a robust network of hydrogen bonds between the lone pairs (LP) on the oxygen atoms of β-CD and the adjacent antibonding orbitals (BD*) of ZA's hydrogen atoms. In the gas phase, the calculated stabilization energies indicated significant charge transfer from β-CD to ZA. Notably, the LP(2) on atom O49 interacted with the BD*(1) of the O151–H169 bond, exhibiting a stabilization energy of 42.10 kcal/mol and a hydrogen bond distance of 1.56 Å. Similar interactions were observed for other β-CD oxygen atoms, such as O65 and O70.

Table 3

Electron donor and acceptor orbitals and the corresponding second-order interaction energy (E^2 (kcal/mol) with NBO (B3LYP-D3/6–31G(d, p)) calculations for configuration A in vacuum and water

Donor	Acceptor	E^2 (kcal/mol)	H-bond (Å)
In vacuum			
	$\beta - CD \rightarrow ZA$		
LP (1) O 49	BD*(1) O 151 - H 169	2.29	1.56
LP (2) O 49	BD*(1) O 151 - H 169	42.10	1.56
LP (2) O 55	BD*(1) O 150 - H 166	4.16	2.23
LP (1) O 61	BD*(1) C 160 - H 165	1.99	2.43
LP (1) O 65	BD*(1) O 153 - H 171	2.35	1.60
LP (2) O 65	BD*(1) O 153 - H 171	36.27	1.60
LP (2) O 70	BD*(1) O 154 - H 172	33.83	1.62
	$ZA \rightarrow \beta - CD$		
LP (1) O 150	BD*(1) O 48 - H 129	9.04	1.97
LP (2) O 153	BD*(1) C 21 - H 100	2.25	2.30
LP (1) O 155	BD*(1) O 69 - H 141	14.74	1.67
LP (3) O 155	BD*(1) O 69 - H 141	15.73	1.67
LP (1) O 156	BD*(1) O 54 - H 132	7.85	1.88
LP (3) O 156	BD*(1) O 54 - H 132	7.54	1.88
LP (1) N 158	BD*(1) O 47 - H 128	20.12	1.87
In water			
	$\beta - CD \rightarrow ZA$		
LP (1) O 49	BD*(1) O 151 - H 169	2.36	1.52
LP (2) O 49	BD*(1) O 151 - H 169	47.14	1.52
LP (2) O 55	BD*(1) O 150 - H 166	2.28	2.39
LP (1) O 61	BD*(1) C 160 - H 165	1.99	2.44
LP (1) O 65	BD*(1) O 153 - H 171	2.63	1.54
LP (2) O 65	BD*(1) O 153 - H 171	45.33	1.54
LP (2) O 70	BD*(1) O 154 - H 172	42.03	1.56
	$ZA \rightarrow \beta - CD$		
LP (1) O 150	BD*(1) O 48 - H 129	9.69	1.94
LP (2) O 153	BD*(1) C 21 - H 100	2.14	2.30
LP (1) O 155	BD*(1) O 69 - H 141	15.50	1.66
LP (3) O 155	BD*(1) O 69 - H 141	17.26	1.66
LP (1) O 156	BD*(1) O 54 - H 132	6.66	1.90
LP (3) O 156	BD*(1) O 54 - H 132	7.56	1.90
LP (1) N 158	BD*(1) O 47 - H 128	24.20	1.83

BD* denotes σ* antibonding orbital, LP denotes valence lone pair; For BD*: (1) denote π orbital; For LP: (1) and (2) denote the first and the second lone pair electron, respectively

In aqueous solution, these interactions were further strengthened, as evidenced by higher stabilization energies and shorter bond distances. For instance, the O49 → BD*(1) (O151–H169)

interaction exhibited an increase in stabilization energy to 47.14 kcal/mol and a reduction in bond distance to 1.52 Å, suggesting that solvation enhances the strength of the hydrogen bonds. Additionally, ZA contributed to the overall stabilization through electron donation to β-CD, as demonstrated by interactions such as LP(3) of O155 → BD*(1) of O69–H141, with a stabilization energy of 15.73 kcal/mol in the gas phase.

QTAIM analysis

QTAIM analysis was applied to configuration A to further explore non-covalent interactions in both gas phase and aqueous environments (Table 4).[42,43] In the gas phase, most interactions were of weak to moderate intensity, with hydrogen bond energies (E_{HB}) ranging from −1.0 to −14.0 kcal/mol. Electron densities at bond critical points (BCPs) ranged from 0.010 to 0.070 a.u., and positive Laplacian values ($\nabla^2\rho(r)$) confirmed the non-covalent nature of the interactions. Total energy densities H(r) close to zero or slightly negative indicated predominantly electrostatic interactions.

Notable interactions included O49 -- H169 (E_{HB} = −13.823 kcal/mol), H171 -- O65 (−12.366 kcal/mol), and H172 -- O70 (−10.963 kcal/mol), all characterized by short distances and high electron densities, underscoring their stabilizing roles.

In aqueous solution, key hydrogen bonds were further strengthened. For example, the O49 -- H169 interaction showed increased E_{HB} (−15.190 kcal/mol) and a reduced bond distance (1.524 Å). Similarly, H171 -- O65 exhibited increased electron density and bonding energy (E_{HB} = −14.715 kcal/mol), reflecting enhanced stabilization in solvent. Conversely, weaker interactions such as O55 -- H166 showed reduced ρ(r) and E_{HB} in aqueous solution, indicating diminished stabilizing contributions.

Overall, both environments are dominated by electrostatic forces, as confirmed by the positive $\nabla^2\rho(r)$ values and near-zero H(r) values. Solvation enhances primary hydrogen bonds while attenuating secondary ones, thus promoting complex stability by reinforcing key interactions.

NCI-RDG and IGM analysis

To further investigate the non-covalent forces stabilizing the ZA@β-CD complex (Configuration A), the NCI-RDG and IGM methods were applied. Results, presented as isosurfaces and scatter plots, compared gas-phase and aqueous environments.[44-46]

NCI-RDG isosurfaces (Fig. 5), colored according to the sign(λ_2)ρ parameter, revealed the nature and intensity of interactions. Key observations include:

- Sign(λ_2)ρ values ranging from −0.05 to +0.02 a.u.;
- RDG maxima reaching ~2.0 a.u., with density clustering around sign(λ_2)ρ ≈ 0, indicating a dominance of weak dispersion interactions;
- Blue regions (sign(λ_2)ρ < −0.02 a.u.) corresponding to weak hydrogen bonds; green regions (−0.02 < sign(λ_2)ρ < +0.01 a.u.) to van der Waals interactions; and red regions (sign(λ_2)ρ > +0.01 a.u.) to steric repulsion, which remained minimal.

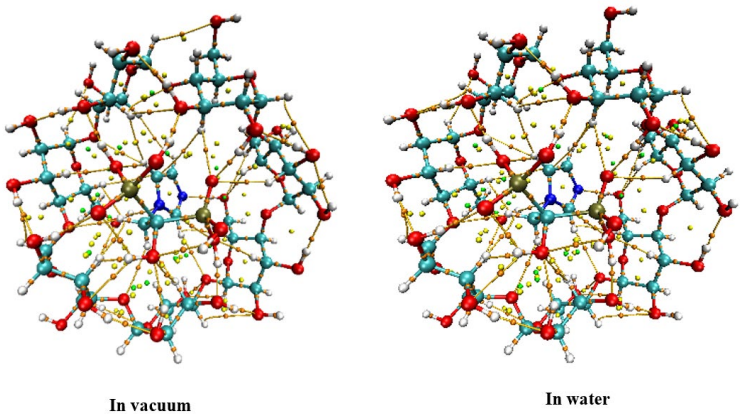

Figure 4: Molecular topography analysis of ZA@β-CD (Configuration A)

Table 4
Topological parameters computed by QTAIM for configuration A in vacuum and water

Interactions	d(Å)	ρ(r)	$\nabla^2\rho(r)$	G(r)	V(r)	H(r)	E_{HB}	Strength	Major nature
In vacuum									
129(H) -- 150(O)	1.97019	0.02358	0.07036	0.01814	-0.01869	-0.00055	-4.518	Weak to medium	Electrostatics
55(O) -- 166(H)	2.23014	0.01594	0.05204	0.01297	-0.01294	0.00004	-2.814	Weak to medium	Electrostatics
49(O) -- 169(H)	1.55964	0.06529	0.15848	0.0485	-0.05738	-0.00888	-13.823	Weak to medium	Electrostatics
88(H) -- 164(H)	1.98686	0.01033	0.03476	0.00745	-0.0062	0.00124	-1.562	Very weak	Dispertion + Electrostatics
93(H) -- 165(H)	1.98418	0.0133	0.04983	0.010435	-0.00841	0.00202	-2.225	Very weak	Dispertion + Electrostatics
132(H) -- 156(O)	1.88326	0.02751	0.08103	0.02034	-0.02043	-0.00008	-5.395	Weak to medium	Electrostatics
81(H) -- 151(O)	2.32053	0.01267	0.03987	0.00955	-0.00913	0.00042	-2.084	Very weak	Dispertion + Electrostatics
61(O) -- 165(H)	2.43349	0.01049	0.03347	0.00787	-0.00738	0.0005	-1.598	Very weak	Dispertion + Electrostatics
168(H) -- 83(H)	2.08989	0.00952	0.03834	0.00747	-0.00535	0.00212	-1.381	Very weak	Dispertion + Electrostatics
100(H) -- 153(O)	2.29659	0.01413	0.04184	0.01038	-0.0103	0.00008	-2.410	Very weak	Dispertion + Electrostatics
155(O) -- 141(H)	1.67035	0.04563	0.14389	0.03604	-0.03611	-0.00007	-9.437	Weak to medium	Electrostatics
137(H) -- 157(N)	2.60578	0.00812	0.03113	0.00658	-0.00537	0.00121	-1.069	Very weak	Dispertion + Electrostatics
158(N) -- 128(H)	1.86652	0.03562	0.08702	0.02278	-0.02381	-0.00103	-7.204	Weak to medium	Electrostatics
155(O) -- 141(H)	1.67035	0.04563	0.14389	0.03604	-0.03611	-0.00007	-9.437	Weak to medium	Electrostatics
171(H) -- 65(O)	1.6016	0.05876	0.15145	0.04338	-0.04889	-0.00552	-12.366	Weak to medium	Electrostatics
172(H) -- 70(O)	1.61583	0.05247	0.14871	0.03939	-0.04161	-0.00222	-10.963	Weak to medium	Electrostatics
155(O) -- 114(H)	2.36082	0.01213	0.04611	0.01016	-0.00879	0.00137	-1.964	Very weak	Dispertion + Electrostatics
In water									
129(H) -- 150(O)	1.9438	0.02452	0.07431	0.01896	-0.01935	-0.00038	-4.728	Weak to medium	Electrostatics
55(O) -- 166(H)	2.38638	0.01175	0.04446	0.01029	-0.00947	0.00082	-1.879	Very weak	Dispertion + Electrostatics
49(O) -- 169(H)	1.52445	0.07142	0.15756	0.05271	-0.06603	-0.01332	-15.190	Medium	Electrostatics
93(H) -- 150(O)	2.41958	0.01242	0.04552	0.01025	-0.00911	0.00113	-2.028	Very weak	Dispertion + Electrostatics
88(H) -- 164(H)	2.02961	0.00931	0.0322	0.00673	-0.00542	0.00132	-1.335	Very weak	Dispertion + Electrostatics
93(H) -- 165(H)	2.09257	0.01069	0.04126	0.00831	-0.0063	0.00201	-1.642	Very weak	Dispertion + Electrostatics
132(H) -- 156(O)	1.90457	0.0268	0.07587	0.01939	-0.01981	-0.00042	-5.236	Weak to medium	Electrostatics
81(H) -- 151(O)	2.3599	0.01172	0.03682	0.00876	-0.00831	0.00044	-1.872	Very weak	Dispertion + Electrostatics
61(O) -- 165(H)	2.43941	0.01025	0.03283	0.00769	-0.00718	0.00052	-1.544	Very weak	Dispertion + Electrostatics
168(H) -- 83(H)	2.02804	0.01048	0.04121	0.00822	-0.00614	0.00208	-1.596	Very weak	Dispertion + Electrostatics
137(H) -- 157(N)	2.65851	0.0069	0.02559	0.00539	-0.00438	0.00101	-0.797	Very weak	Dispertion + Electrostatics
100(H) -- 153(O)	2.30342	0.0138	0.04185	0.01026	-0.01006	0.0002	-2.336	Very weak	Dispertion + Electrostatics
155(O) -- 141(H)	1.65595	0.04741	0.14784	0.03742	-0.03789	-0.00046	-9.834	Weak to medium	Electrostatics
158(N) -- 128(H)	1.83403	0.0388	0.09204	0.02451	-0.026	-0.0015	-7.913	Weak to medium	Electrostatics
171(H) -- 65(O)	1.53666	0.06929	0.15579	0.05084	-0.06274	-0.0119	-14.715	Medium	Electrostatics
172(H) -- 70(O)	1.55811	0.06188	0.15566	0.04584	-0.05277	-0.00693	-13.062	Weak to medium	Electrostatics
155(O) -- 14(H)	2.38413	0.01177	0.04319	0.00964	-0.00848	0.00116	-1.883	Very weak	Dispertion + Electrostatics

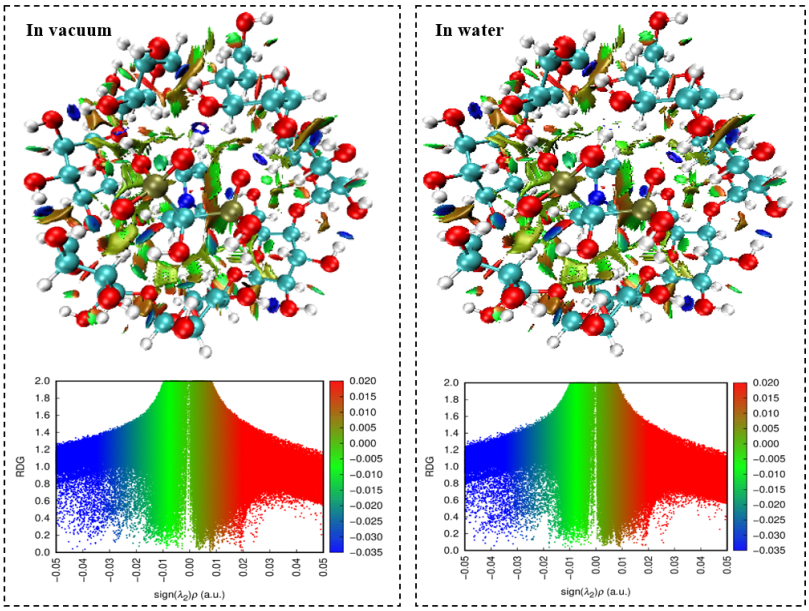

Figure 5: Scatter plots together with the color-filled NCI-RDG isosurfaces of ZA@β-CD (Configuration A)

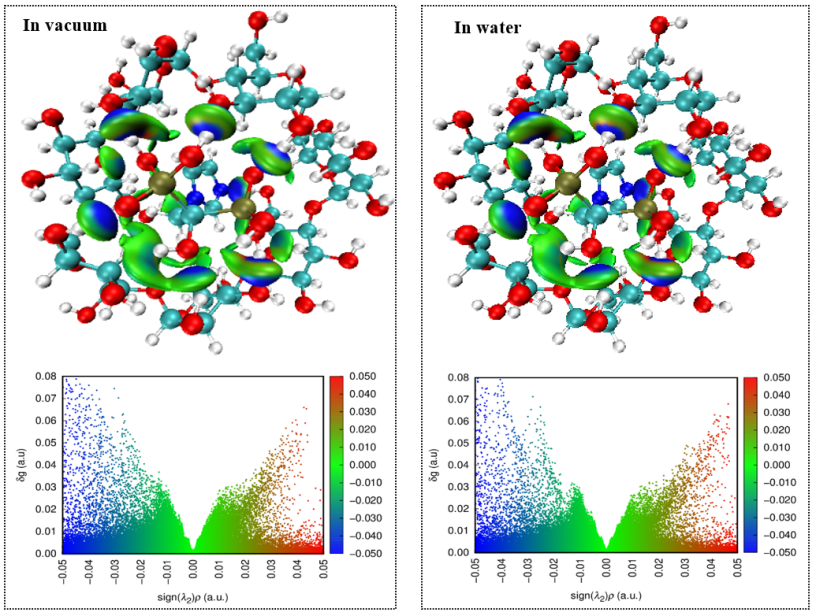

Figure 6: IGM isosurfaces and scatter plots of ZA@β-CD (Configuration A)

Van der Waals interactions (green zones) were consistently observed within the β-CD cavity in both environments. In the gas phase, these zones were more diffuse, while in aqueous solution they appeared more confined. Blue regions near heteroatoms (oxygen and nitrogen) confirmed weak, but stabilizing hydrogen bonds.

IGM analysis (Fig. 6) corroborated these findings by identifying regions where electronic density deviates from non-interacting fragments, signaling weak but relevant interactions. The isosurfaces, also colored by sign(λ_2)ρ, showed a dominance of green zones at the ZA–β-CD interface (dispersion forces) and blue areas near polar groups (hydrogen bonding), while red zones (steric clashes) were negligible.

IGM-derived scatter plots confirmed these interactions, with sign(λ_2)ρ values between −0.05 and +0.05 a.u. and a peak interaction intensity around 0.08 a.u. These findings establish dispersion as the primary stabilizing force in the ZA@β-CD complex, with hydrogen bonding playing a supportive but secondary role. The similarity of interaction profiles across both phases

demonstrates the structural robustness of the complex regardless of the medium.

^{1}H NMR GIAO/DFT calculations

The variations in the ^{1}H NMR chemical shifts of both ZA and β-CD, induced by the formation of the ZA@β-CD inclusion complex, were investigated using theoretical NMR calculations. The GIAO method was applied within the Gaussian 09 package, at the B3LYP-D3/6-31G(d,p) level of theory. Tetramethylsilane (TMS) served as the calibration reference, and solvent effects were incorporated using the CPCM configuration with water as the solvent (ε = 78.35). The theoretical chemical shifts alongside available experimental data[9] for the isolated molecules (ZA and β-CD) and their most stable complex (ZA@β-CD) are presented in Table 5.

Comparative analysis between theoretical and experimental data revealed notable changes in proton resonances for both host and guest molecules, reflecting alterations in the electronic environment upon complexation.[47,48] For ZA, the most pronounced shifts occurred for protons H1, H3, and H6. For instance, the chemical shift of H1 increased from 7.602 ppm (free form) to 8.283 ppm in the complex (Δδ = 0.681 ppm), while H3 showed a larger shift of 1.205 ppm. These variations indicate specific interactions likely hydrogen bonding and conformational rearrangement between these protons and the β-CD cavity.

In β-CD, significant changes were observed for protons H5 and H6, which are located at the inner edge of the cavity. The H5 signal shifted from 3.786 ppm to 4.423 ppm (Δδ = 0.637 ppm), while H6 moved from 4.409 ppm to 4.154 ppm (Δδ = 0.255 ppm). Additionally, the H7 and H8 signals shifted downfield by 1.279 ppm and 3.400 ppm, respectively, reinforcing the occurrence of host–guest interactions and guest encapsulation.

The good agreement between calculated and experimental chemical shifts strongly validates the theoretical configuration and confirms the successful formation of the ZA@β-CD inclusion complex. These spectroscopic variations indirectly but convincingly support the presence of hydrogen bonds and the effectiveness of the complexation process.

Table 5
Theoretical chemical shifts results calculated by B3LYP-D3/6–31G(d, p) (ppm)
in comparison with experimental data

Chemical shifts	Zaledronic	Complex ZA@β-CD	/ΔδZA/	β-CD	Complex ZA@β-CD	/Δ δ β-CD/
H1	7.602 (8.798)	8.283 (8.807)	0.681 (0.009)	3.786 (4.774)	6.082 (4.779)	2.296 (0.005)
H2	7.948 (7.416)	7.281 (7.411)	0.667 (0.005)	4.089 (3.316)	3.855 (3.322)	0.234 (0.006)
H3	7.357 (7.552)	8.562 (7.554)	1.205 (0.002)	3.039 (3.710)	4.154 (3.787)	1.115 (0.077)
H4	4.77 (4.473)	4.833 (4.482)	0.063 (0.009)	4.089 (3.251)	3.411 (3.224)	0.678 (0.027)
H5	5.427 (8.216)	5.673 (8.269)	0.246 (0.053)	3.786 (3.572)	4.423	0.637
H6	11.431 (15.362)	11.272 (15.423)	0.159 (0.061)	4.409 (4.518)	4.154 (4.492)	0.255 (0.026)
H7				4.803 (3.584)	6.082	1.279
H8				2.455 (5.663)	5.855 (5.719)	3.400 (0.056)
H9				3.786 (5.728)	3.411 (5.780)	0.375 (0.052)

TD-DFT calculations

To explore the photophysical properties and excitation mechanisms of the ZA@β-CD complex, TD-DFT calculations were performed at the B3LYP-D3/6-31G(d,p) level in both gas phase and aqueous solution. Solvent effects were incorporated using the CPCM configuration. The calculated excitation energies (E), wavelengths (λ), oscillator strengths (f), and orbital contributions are detailed in Table 6.

Gas phase results:

The simulated absorption spectrum of the complex displayed three prominent electronic transitions:

- The first transition, at 204.24 nm (E = 6.071 eV; f = 0.049), corresponds to a locally excited (LE) state on the ZA molecule, predominantly characterized by HOMO–1 → LUMO (62.90%) and HOMO–1 → LUMO+1 (21.80%) transitions.
- The second transition, at 193.59 nm (E = 6.405 eV; f = 0.044), also reflects LE character, mainly from HOMO–1 → LUMO+1 (63.01%) and HOMO–1 → LUMO (19.62%).
- The third transition, at 169.39 nm (E = 7.320 eV; f = 0.019), exhibits charge transfer (CT) character from β-CD to ZA, involving HOMO–11 → LUMO+1 (33.57%), HOMO–9 → LUMO+1 (10.44%), and a minor LE contribution from HOMO–1 → LUMO+3 (12.81%).

Aqueous phase results:

In the presence of water, the excitation profile shifted notably, with an increased CT component:

- The most intense transition at 204.23 nm (E = 6.071 eV; f = 0.032) shows a mixed LE/CT character, with HOMO → LUMO (58.84%, LE on ZA) and HOMO–1 → LUMO (33.93%, CT).
- A nearby transition at 203.99 nm (E = 6.078 eV; f = 0.038) is dominated by HOMO–1 → LUMO (60.40%, CT from β-CD to ZA) and HOMO → LUMO+1 (17.17%, LE).
- The third transition at 193.86 nm (E = 6.396 eV; f = 0.066) retains a predominantly LE character, driven by HOMO → LUMO+1 (63.54%) and HOMO → LUMO (19.33%).

These observations highlight the key role of solvent polarity in modulating the electronic properties of the complex. In the gas phase, transitions are mainly local, whereas in aqueous media, charge transfer becomes more prominent, indicating stronger electronic communication between host and guest. This enhanced orbital delocalization in polar environments contributes to the supramolecular stability of the complex and underlines its potential in light-driven applications, particularly for targeted drug delivery. The TD-DFT results (illustrated in Fig. 7) confirm that ZA@β-CD is a photoactive and electronically stable supramolecular system, capable of intracomplex electron transfer, and suitable for applications in photochemistry.

Additionally, the theoretical UV–Vis absorption spectrum shows good agreement with the experimentally obtained spectrum of the ZA@β-CD complex.

Table 6
Wavelengths of absorption bands (λ), excitation energies (E), oscillator strengths (f), light-harvesting efficiency (LHE (%)), and orbital contributions in aqueous solution for model A

	λ (nm)	E (eV)	f	LHE (%)	Minor and major orbital contribution		Nature of excited states
In vacuum	204.24	6.071	0.049	10.60	62.90%	(HOMO-1) → (LUMO)	LE(ZA)
					21.80%	(HOMO-1) → (LUMO+1)	LE(ZA)
	193.59	6.405	0.044	9.60	19.62%	(HOMO-1) → (LUMO)	LE(ZA)
					63.01%	(HOMO-1) → (LUMO+1)	LE(ZA)
	169.39	7.320	0.019	4.19	33.57%	(HOMO-11) → (LUMO+1)	CT(CD→ZA)
					10.44%	(HOMO-9) → (LUMO+1)	CT(CD→ZA)
					12.81%	(HOMO-1) → (LUMO+3)	LE(ZA)
In water	204.23	6.071	0.032	7.17	33.93%	(HOMO-1) → (LUMO)	CT(CD→ZA)
					58.84%	(HOMO) → (LUMO)	LE(ZA)
	203.99	6.078	0.038	8.33	60.40%	(HOMO-1) → (LUMO)	CT(CD→ZA)
					17.17%	(HOMO) → (LUMO+1)	LE(ZA)
	193.86	6.396	0.066	14.10	19.33%	(HOMO) → (LUMO)	LE(ZA)
					63.54%	(HOMO) → (LUMO+1)	LE(ZA)
					63.54%	(HOMO) → (LUMO+1)	LE(ZA)

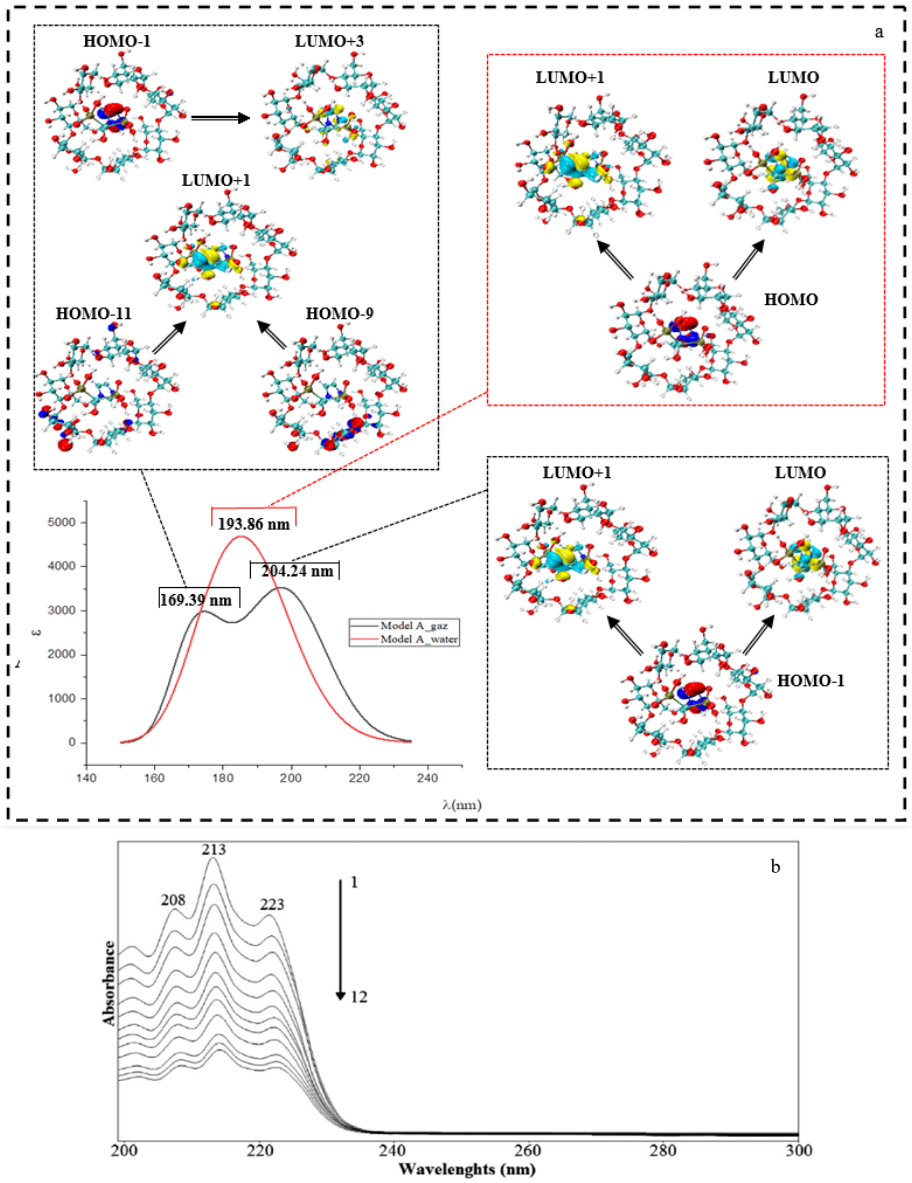

Figure 7: UV-Vis absorption spectra of the ZA@β-CD inclusion complex: (a) Theoretical TD-DFT spectrum computed in the aqueous phase; (b) Experimental spectrum, reproduced from Dikmen[9]

The experimental data reveal characteristic absorption peaks around 208, 213, and 223 nm, which are accurately reproduced by the calculated electronic transitions, with only minor deviations attributed to solvent effects and the inherent limitations of the TD-DFT method.

To provide deeper insight into the photophysical properties of the ZA@β-CD complex, the light-harvesting efficiency (LHE) was evaluated using the equation LHE = $(1 - 10^{-f}) \times 100\%$. As presented in Table 6, the LHE values exhibit substantial variation, depending on the characteristics of the electronic transition and the surrounding environment. The computational results reveal that LHE values range from 4.19% to 10.60% in the gas phase. In contrast, in aqueous solution, the values are notably higher, spanning from 7.17% to 14.10%. This increase suggests that solvent interactions enhance the light-harvesting capacity of the system by promoting orbital delocalization and reinforcing host–guest electronic interactions.

Notably, the most intense electronic transitions correspond to higher oscillator strengths, which, in turn, lead to an improvement in the LHE, particularly for excitations occurring in the aqueous phase. This observation underscores the favorable influence of polar solvents on the photoresponse properties of the ZA@β-CD inclusion complex.

MC docking simulations

MC docking simulations were performed to examine the mechanism of ZA insertion into the β-CD cavity.[49-51] These simulations enabled a comprehensive mapping of the conformational space and yielded thermodynamic descriptors reflecting the supramolecular system's behavior.

The configurations were constructed using the Amber 99 force field,[52] which is particularly effective for simulating large macromolecules like β-CD. The simulation procedure was structured into three sequential stages, each designed to provide a deeper understanding of the system's energy evolution:

- Phase I (trials 1–35,000): A rapid decrease in potential energy was observed, indicating the progressive approach of the ZA molecule toward the β-CD cavity;
- Phase II (trials 35,000–100,000): The system reached an energy plateau, where the minimum potential and complexation energies indicated deeper penetration of the guest into the host cavity and a thermodynamically stable conformation;
- Phase III (after trial 100,000): Stabilization of potential energy signaled equilibrium and the formation of a stable complex.

The gas-phase energy data for both configurations are summarized in Table 7. Potential energy profiles for the insertion of ZA into β-CD (Configurations A and B) are shown in Figure 8, with calculated energies represented by the black curve and interpolated values by the red curve.

Table 7
Computed potential energy, complexation energy, interaction energy, and deformation energy from Monte Carlo docking simulations of the zoledronic acid@β-cyclodextrin complex in the gas phase

	⟨Ep⟩[a]	ΔE_C	E_{int}	E_{def} (ZA)	E_{def} (β-CD)
Configuration A	36.35	- 29.91	- 33.15	0.55	0.89
Configuration B	49.86	- 26.65	- 29.53	0.41	0.64
ΔE[b]	13.51	3.26	3.62	-0.14	-0.25

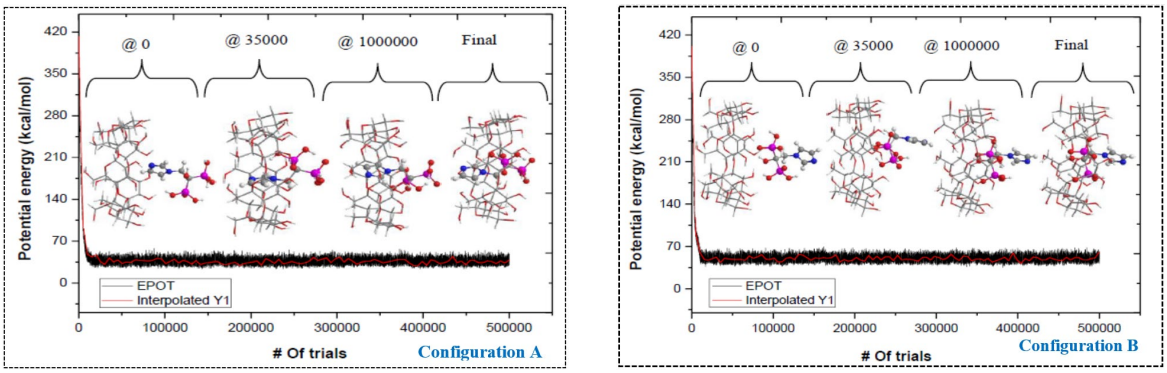

Figure 8: Calculated potential energy curves in MC simulations of zoledronic acid docking in β-CD in gas for configurations A and B (potential energy curve (black) and interpolated values (red))

Mean energy comparisons reveal that configuration A exhibits lower values than configuration B for potential energy, complexation energy, and interaction energy. The respective energy differences between configurations A and B were 13.51 kcal/mol (potential), 3.26 kcal/mol (binding), and 3.62 kcal/mol (interaction), all favoring configuration A.

Another key observation pertains to host deformation energy: β-CD exhibited consistently higher deformation energies than the guest (ZA), regardless of the configuration. This highlights the importance of β-CD's conformational flexibility, which is essential for structural adaptation and the formation of a stable inclusion complex.

CONCLUSION

This comprehensive theoretical study provides detailed insights into the structural, energetic, and electronic properties of the zoledronic acid (ZA) inclusion complex with β-cyclodextrin (β-CD). A multi-level computational approach was employed, integrating PM6-D3H4, DFT-D3, TD-DFT, NBO, QTAIM, NCI-RDG, IGM, and Monte

Carlo (MC) simulations, to assess the thermodynamic stability and interaction mechanisms of the ZA@β-CD complex in both gas and aqueous phases.

The results indicate that the formation of the ZA@β-CD complex is thermodynamically favorable, with configuration A, where the imidazole group of ZA is inserted through the wider rim of β-CD, demonstrating superior stability across all configurations studied. Non-covalent interactions, particularly hydrogen bonds and dispersion forces, were identified as key contributors to the stabilization of the complex. Notably, solvation effects enhanced hydrogen bonding and promoted host–guest complementarity.

QTAIM and NBO analyses provided evidence for significant donor–acceptor interactions, while RDG and IGM analyses mapped the spatial distribution of non-covalent forces within the β-CD cavity. The TD-DFT analysis revealed distinct charge-transfer and locally excited states, with solvent polarity influencing the excitation profiles and enhancing electron delocalization across the complex.

Theoretical NMR chemical shift calculations yielded a strong correlation with experimental data, thus validating the proposed configuration and confirming the successful inclusion of ZA into the β-CD cavity. Furthermore, MC docking simulations corroborated the energetic favorability and conformational flexibility of the complex, reaffirming the stability of configuration A.

Overall, this study provides a deeper molecular-level understanding of the ZA@β-CD inclusion complex, offering valuable insights into its potential for improving the solubility, stability, and delivery efficiency of zoledronic acid in pharmaceutical applications. These findings underscore the promise of cyclodextrin-based inclusion complexes as effective drug delivery strategies in the formulation of bioactive compounds.

REFERENCES

[1] M. Vassaki, S. Lazarou, P. Turhanen, D. Choquesillo-Lazarte and K. D. Demadis, *Molecules*, **27**, 6212 (2022), https://doi.org/10.3390/molecules27196212

[2] C. M. Perry and D. P. Figgitt, *Drugs*, **64**, 1197 (2004), https://doi.org/10.2165/00003495-200464110-00004

[3] K. Wellington and K. L. Goa, *Drugs*, **63**, 417 (2003), https://doi.org/10.2165/00003495-200363040-00009

[4] R. G. Russell, *Bone*, **49**, 2 (2011), https://doi.org/10.1016/j.bone.2011.04.022

[5] M. T. Drake, B. L. Clarke and S. Khosla, *Mayo Clin. Proc.*, **83**, 1032 (2008), https://doi.org/10.4065/83.9.1032

[6] F. L. Lanza, *Mol. Diagn. Ther.*, **1**, 37 (2002), https://doi.org/10.2165/00024677-200201010-00004

[7] M. Tadrous, L. Wong, M. M. Mamdani, D. N. Juurlink, M. D. Krahn *et al.*, *Osteoporos. Int.*, **25**, 1225 (2014), https://doi.org/10.1007/s00198-013-2576-2

[8] J. Biernacka, K. Betlejewska-Kielak, J. Witowska-Jarosz, E. Klosińska-Szmurlo and A. P. Mazurek, *J. Incl. Phenom. Macrocycl. Chem.*, **78**, 437 (2014), https://doi.org/10.1007/s10847-013-0315-0

[9] G. Dikmen, *J. Mol. Struct.*, **1261**, 132897 (2022), https://doi.org/10.1016/j.molstruc.2022.132897

[10] W. Bouneb, A. Bouhadiba, N. Naili, A. Benaissa, M. Rahim *et al.*, *Chem. Afr.*, **8**, 1937 (2025), https://doi.org/10.1007/s42250-025-01264-6

[11] H. Chekroud, A. Bouhadiba, N. Naili, A. Benaïssa, F. Djazi *et al.*, *Russ. J. Org. Chem.*, **61**, 162 (2025), https://doi.org/10.1134/S1070428024603297

[12] A. Fifere, M. Spulber, N. Marangoci, N. Fifere, M. Pinteala *et al.*, *Cellulose Chem. Technol.*, **45**, 149 (2011), https://www.cellulosechemtechnol.ro/pdf/CCT3-4(2011)/p.149-156.pdf

[13] F. Chekkal, N. Naili, A. Benaïssa, M. A. Zerizer and B. Zouchoune, *Struct. Chem.*, **35**, 1539 (2024), https://doi.org/10.1007/s11224-024-02300-w

[14] N. Naili, A. Benaïssa, F. Chekkal, M. A. Zerizer, B. Zouchoune *et al.*, *Struct. Chem.*, **36**, 527 (2025), https://doi.org/10.1007/s11224-024-02383-5

[15] M. J. Frisch, G. W. Trucks, H. B. Schlegel, G. E. Scuseria, M. A. Robb *et al.*, Gaussian 09 Revision A.1, Gaussian, Inc., Wallingford (2009)

[16] R. Dennington, T. Keith and J. M. Millam, GaussView (Version 6.1.1). Semichem Inc. Shawnee Mission, KS (2016)

[17] Hyperchem Release 7.51 for Windows, Hypercube Inc., Hyperchem 7.5 (2002)

[18] Chem-Oce 3D ultra, (2006) Version 10, Cambridge Software

[19] J. J. P. Stewart, "Stewart Computational Chemistry", MOPAC, Colorado Springs, USA, 2016, http://OpenMOPAC.net

[20] L. Liu and Q. X. Guo, *J. Incl. Phenom. Macrocycl. Chem.*, **50**, 95 (2004), https://doi.org/10.1007/s10847-003-8847-3

[21] A. D. Becke, *J. Chem. Phys.*, **98**, 5648 (1993), https://doi.org/10.1063/1.464913

[22] C. Lee, W. Yang and R. G. Parr, *Phys. Rev. B*, **37**, 785 (1988), https://doi.org/10.1103/PhysRevB.37.785

[23] M. M. Francl, W. J. Pietro, W. J. Hehre, J. S. Binkley, M. S. Gordon *et al.*, *J. Chem. Phys.*, **77**, 3654 (1982), https://doi.org/10.1063/1.444267

[24] V. Barone and M. Cossi, *J. Phys. Chem. A*, **102**, 1995 (1998), https://doi.org/10.1021/jp9716997

[25] P. Cantero-López, J. Sánchez, M. S. P. Meza, C. A. García-Negrete and O. Yáñez, *Chem. Phys.*, **588**, 112483 (2025), https://doi.org/10.1016/j.chemphys.2024.112483
[26] T. Lu and Q. Chen, *Compr. Comput. Chem.*, **2**, 240 (2024), https://doi.org/10.1016/B978-0-12-821978-2.00076-3
[27] T. Lu and Q. Chen, *J. Comput. Chem.*, **43**, 539 (2022), https://doi.org/10.1002/jcc.26812
[28] A. E. Reed, L. A. Curtiss and F. Weinhold, *Chem. Rev.*, **88**, 899 (1988), https://doi.org/10.1021/cr00088a005
[29] F. Weinhold, C. Landis and E. Glendening, *Int. Rev. Phys. Chem.*, **35**, 399 (2016), https://doi.org/10.1080/0144235X.2016.1192262
[30] E. R. Johnson, S. Keinan, P. Mori-Sánchez, J. Contreras-García, A. J. Cohen *et al.*, *J. Am. Chem. Soc.*, **132**, 6498 (2010), https://doi.org/10.1021/ja100936w
[31] J. Contreras-García, E. R. Johnson, S. Keinan, R. Chaudret, J. P. Piquemal *et al.*, *J. Chem. Theory Comput.*, **7**, 625 (2011), https://doi.org/10.1021/ct100641a
[32] R. F. W. Bader, "Atoms in Molecules—A Quantum Theory", Clarendon Press, Oxford, 1990
[33] T. Helgaker, M. Jaszunski and K. Ruud, *Chem. Rev.*, **99**, 293 (1999), https://doi.org/10.1021/cr960017t
[34] T. Lu and F. Chen, *J. Comput. Chem.*, **33**, 580 (2012), https://doi.org/10.1002/jcc.22885
[35] T. Lu, *J. Chem. Phys.*, **161**, 082503 (2024), https://doi.org/10.1063/5.0216272
[36] W. Humphrey, A. Dalke and K. Schulten, *J. Mol. Graph.*, **14**, 33 (1996), https://doi.org/10.1016/0263-7855(96)00018-5
[37] S. J. Weiner, P. A. Kollman, D. T. Nguyen and D. A. Case, *J. Comput. Chem.*, **7**, 230 (1986), https://doi.org/10.1002/jcc.540070216
[38] D. A. Pearlman, D. A. Case, J. W. Caldwell, W. S. Ross, T. E. Cheatham *et al.*, *Comput. Phys. Commun.*, **91**, 1 (1995), https://doi.org/10.1016/0010-4655(95)00041-D
[39] P. Bonnet, I. Beà, C. Jaime and L. Morin-Allory, *Supramol. Chem.*, **15**, 251 (2003), https://doi.org/10.1080/1061027031000140176
[40] S. Kumar, B. H. Kumar, R. Nayak, S. Pandey, N. Kumar *et al.*, *Mol. Divers.*, **29**, 5607 (2025), https://doi.org/10.1007/s11030-024-11075-5
[41] A. I. Ramos, T. M. Braga, P. Silva, J. A. Fernandes, P. Ribeiro-Claro *et al.*, *CrystEngComm.*, **15**, 2822 (2013), https://doi.org/10.1039/C3CE26414A
[42] L. Leherte, T. Latour and D. P. Vercauteren, *Supramol. Sci.*, **2**, 209 (1995), https://doi.org/10.1016/0968-5677(96)89677-5
[43] P. S. V. Kumar, V. R. Vendra and V. Subramanian, *J. Chem. Sci.*, **128**, 1527 (2016), https://doi.org/10.1007/s12039-016-1172-3
[44] C. Lefebvre, G. Rubez, H. R. Khartabil, J. C. Boisson, J. Contreras-García *et al.*, *Phys. Chem. Chem. Phys.*, **19**, 17928 (2017), https://doi.org/10.1039/C7CP02110K
[45] F. A. Messiad, N. Ammouchi, Y. Belhocine, H. Alhussain, M. G. Ghoniem *et al.*, *Nanomaterials*, **12**, 2517 (2022), https://doi.org/10.3390/nano12152517
[46] Z. Kabouche, Y. Belhocine, T. Benlecheb, I. M. Assaba, A. Litim *et al.*, *Chim. Techn. Acta*, **10**, 202310209 (2023), https://doi.org/10.15826/chimtech.2023.10.2.09
[47] H. F. Dos Santos, E. P. Ávila and C. P. A. Anconi, *Aust. J. Chem.*, **78**, CH24150 (2025), https://doi.org/10.1071/CH24150
[48] Y. Belhocine, A. Bouhadiba, M. Rahim, L. Nouar, I. Djilani *et al.*, *Macroheterocycles*, **11**, 203 (2018), https://doi.org/10.6060/mhc170829b
[49] H. Kim, K. Jeong, H. Park and S. Jung, *J. Incl. Phenom. Macrocycl. Chem.*, **54**, 165 (2006), https://doi.org/10.1007/s10847-005-6288-x
[50] N. Mekarba, F. Krid, Y. Belhocine, A. Bouhadiba, S. Rahali *et al.*, *Theor. Chem. Acc.*, **144**, 3 (2025), https://doi.org/10.1007/s00214-024-03164-3
[51] Y.-H. Choi, C.-H. Yang, H.-W. Kim and S. Jung, *Carbohyd. Res.*, **328**, 393 (2000), https://doi.org/10.1016/S0008-6215(00)00101-4
[52] S. J. Weiner, P. A. Kollman, D. T. Nguyen and D. A. Case, *J. Comput. Chem.*, **7**, 230 (1986), https://doi.org/10.1002/jcc.540070216